Critical currents and microstructure of melt-textured stoichiometric $YBa_2Cu_3O_{7-\delta}$ crystallites

M. Ullrich and D. Müller
Institut für Metallphysik, Hospitalstrasse 3/7, 37073 Göttingen, Federal Republic of Germany

W. Mexner
Zentrum für Funktionswerkstoffe, Windausweg 2, 37073 Göttingen, Federal Republic of Germany

M. Steins
Mineralogisch-Kristallographisches Institut, Goldschmidtstrasse 1, 37073 Göttingen, Federal Republic of Germany

K. Heinemann and H. C. Freyhardt
Institut für Metallphysik, Hospitalstrasse 3/7, 37073 Göttingen, Federal Republic of Germany
(Received 1 March 1993; revised manuscript received 1 June 1993)

To avoid weak-link behavior caused by grain boundaries small crystallites of $YBa_2Cu_3O_{7-\delta}$ were mechanically separated from ~ 1 cm^3 Bridgman-melt-textured blocks. Using the Bean critical-state model, j_c values at 4 K and 5 T (70 K and 2 T) as high as $\sim 2\times 10^6$ A/cm^2 ($\sim 4\times 10^4$ A/cm^2) were estimated from the width of the magnetization hysteresis. Microstructural investigations of the crystallites reveal the existence of dislocations, finely distributed inclusions, stacking faults, twin boundaries, elementary growth steps, and oxygen-deficient regions. The defects are thought to have a strong influence on the pinning behavior and the shape of the magnetization curve.

I. INTRODUCTION

The key parameter for applications of high-temperature superconductors (HTSC) is the critical current density, j_c. Both the intergranular and the intragranular j_c are remarkably raised by melt texturing.[1–7] The enhancement of the intergranular j_{c_i} is mainly due to a texture between the grains and an enlargement of the grains themselves. Thus, the detrimental influence of weak links at grain boundaries[8,9] on the transport critical current density, j_{c_t}, is greatly reduced.

Due to an incomplete peritectic reaction of $Y_2BaCuO_5(s)+3\ BaCuO_2(l)+2CuO(l)\Rightarrow 2\ YBa_2Cu_3O_{7-\delta}(s)$,[10] even at very slow cooling rates of about 1 K/h, Y_2BaCuO_5 (Y 2:1:1) inclusions and (Ba,Cu)-rich phases still remain present after cooling through the peritectic reaction. These nonsuperconducting phases could act as pinning centers and could be one reason for the increase of the intragranular $j_{c,\Delta M}$. Murakami *et al.* reported, that Y 2:1:1 additions to the stoichiometric $YBa_2Cu_3O_{7-\delta}$ (YBCO) precursor could raise j_c even more.[11–13] Nevertheless, whether Y 2:1:1 acts as a grain boundary cleaner by removing the excess (Ba,Cu)-rich solidified liquid from the grain boundaries or as a pinning center inside the grains is still under discussion.

In this study we used small crystallites of YBCO to avoid any ambiguity due to weak-link behavior of grain boundaries. The microstructure and magnetization behavior of the crystallites were investigated to reveal the nature of the high-$j_{c,\Delta M}$ values in this material.

II. EXPERIMENT

The melt-textured samples were prepared by slowly cooling stoichiometric YBCO pellets through the peritectic reaction as shown schematically in Fig. 1. For the melt-texturing a modified three-zone Bridgman furnace was employed with a fixed thermal gradient of 25 K/cm. To ensure a high oxygen partial pressure, p_{O_2}, the samples were sealed in a quartz tube. In general p_{O_2} (1000 °C) ≥ 1 bar was selected. Details of the sample preparation are given in Ref. 14. From the resulting ~ 1 cm^3 blocks small crystallites with dimensions of about $500\times 500\times 50$ μm^3 were mechanically separated. Deviations of the exact stoichiometric composition of $YBa_2Cu_3O_{7-\delta}$ were estimated by electron microprobe

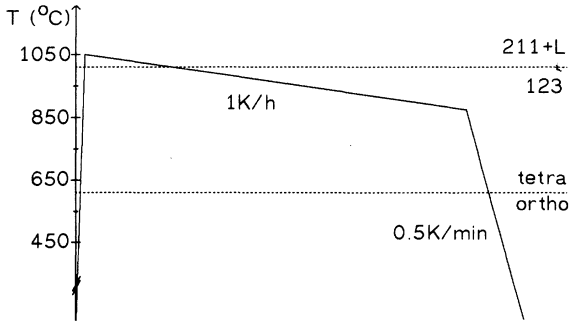

FIG. 1. Schematic drawing of the temperature profile used in the melt-texturing process.

analysis (EPMA). T_c of the crystallites was measured by ac susceptibility. Structure and orientation of the samples were determined by means of a four-circle x-ray diffractometer using Mo $K\alpha$ radiation, by an analytical scanning electron microscope (SEM) detecting secondary electrons as well as backscattering electrons and by an optical microscope. The surface of the crystallites was investigated by a scanning tunneling microscope (STM) and their microstructure by means of a transmission electron microscope (TEM). Two kinds of TEM sample preparation have been used, i.e., crushing and ion milling. In order to minimize preparation-induced defects the samples were cooled with liquid nitrogen during thinning, but also during the TEM observations themselves. Magnetization measurements were performed in external magnetic fields up to 10 T between 4 K and T_c using a Faraday balance with a chosen magnetic-field gradient of 1 T/m. The external magnetic field was oriented parallel to the c axis. Critical current densities were evaluated from the hysteric magnetization curves by applying the anisotropic Bean model[15,16] and by using demagnetization factors, D, which were estimated from the initial slope of the virgin curves for very small fields.

III. RESULTS

A. XRD measurements

To check orientation and the quality of the crystallites, x-ray-diffraction (XRD) measurements with Mo $K\alpha$ radiation were performed by means of a four-circle diffractometer. Texture scans of different reflections were performed similar to texture scans of thin films[17,18] in order to look for different domains as a function of the direction. Therefore, χ and ϕ scans were done using fixed 2Θ and ω of the Bragg condition. A scan of the (005) reflection [Fig. 2(a)] reveals that one does not find different domains with nonparallel ab planes. On the other hand, in most of the crystallites, patterns of reflections which are different from (001) exhibit a splitting as in the case of the (103)/(013) reflection of Fig. 2(b). Nevertheless, the angle between the two maxima is always less than 1°. Therefore, either only two domains with one small-angle grain boundary exist in this crystallite or there are n domains with $n-1$ small-angle grain boundaries always of the same angle. From XRD measurements it is impossible to conclude how the domains are oriented with respect to each other. First, because we do not see any orientation contrast at the surface of the crystallites using a SEM in the backscattering mode and second, because we often observe moiré patterns[19] in TEM investigations of the crystallites,[14] we assume the crystallites to be built up by stacking up different domains consisting of "quasi single crystallites" which possess a common c axis (Fig. 3).

B. Microstructure

1. TEM

TEM observations reveal the presence of finely distributed inclusions. Their average diameter is about 35 nm and their density, N_i, amounts to about 6×10^{19} m^{-3}. Because of the small diameter of the inclusions, only a few could be identified as $BaCuO_2$ by moiré fringes and electron-diffraction pattern. The striking feature apart from the small size of the inclusions is that they are associated with dislocations (Fig. 4), which could be introduced as well by the high-temperature treatment as by tensions created by lattice parameter differences of the superconducting matrix and the inclusions. The observed dislocation density ($N_d \approx 1-2\times10^{10}$ cm^{-2}) is much higher than in polycrystalline bulk YBCO ($N_d \ll 10^7$ cm^{-2}).[20] The burgers vector, **b**, of the dislocations is a [100], or b [010], where a and b denote the lattice parameters of the YBCO unit cell. In addition we observe twins with average spacings of about 280 nm as well as planar defects like stacking faults.[21]

No significant difference of the microstructure of the differently thinned samples has been observed. Therefore, we assume that these microstructural defects, e.g.,

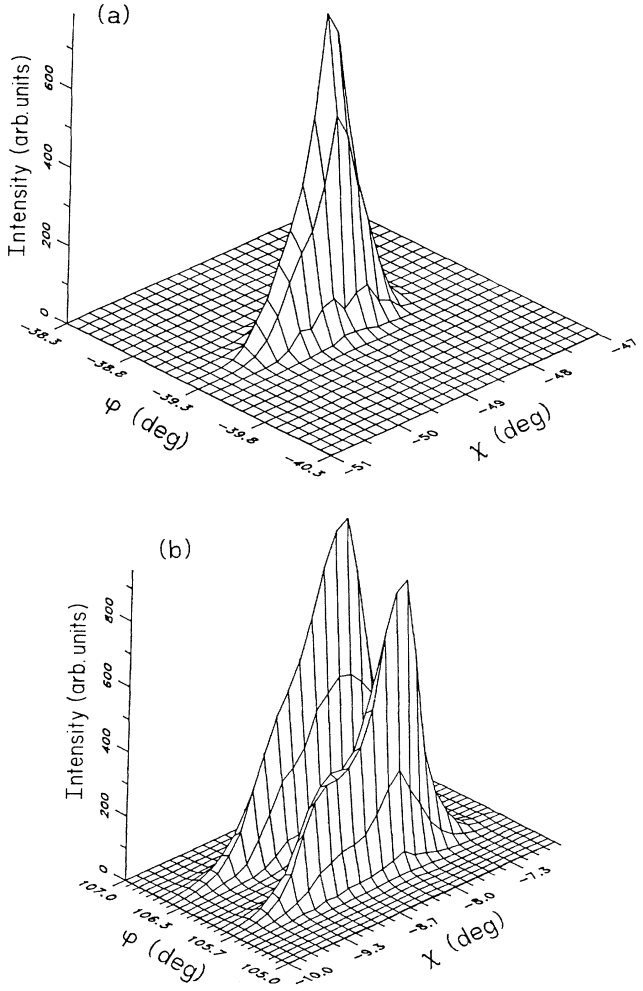

FIG. 2. Texture scans of (a) the (005) and (b) the (013)/(103) reflection. The scans were obtained from the whole crystallite volume.

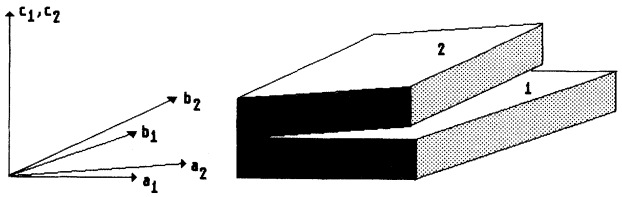

FIG. 3. Schematic drawing of a crystallite, built up by a stack of two "quasi single crystals" with parallel c axis and a slight misorientation of less than 1° in the a and the b axis.

the fine inclusions, are created during the melt-texturing process.

2. *Optical and analytical scanning electron microscopy*

Optical microscopy and SEM investigations of the crystallites reveal smooth surfaces with some large growth steps (Fig. 5) at the edge of the crystallites and twin boundaries over the whole surface of the crystallites. From a SEM image with backscattered electrons (Fig. 6) an average twin spacing of about 270 nm could be estimated which is about the same order of magnitude than obtained by TEM observations.

3. *STM*

Investigations of the surfaces of freshly separated crystallites were performed by means of a STM using mechanically prepared Pt/Ir tips, a tunneling voltage U_{bias} of 800 mV, and a tunneling current I_t of 100 pA. All crystallites exhibit a smooth surface and a regular structure with no imperfections except from growth steps of the height of the elementary unit cell in the c direction [Figs. 7(a) and 7(b)].

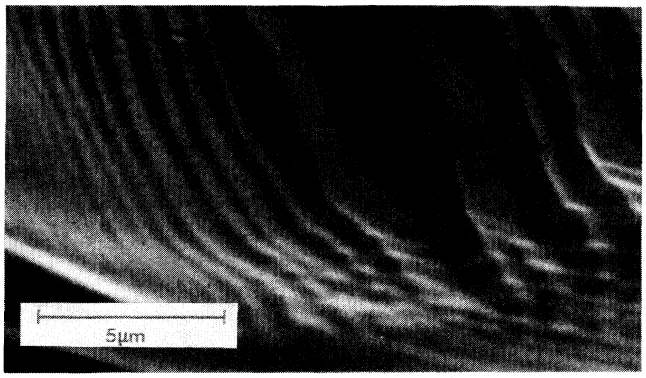

FIG. 5. SEM micrograph of the edge of a crystallite. Large growth steps are visible.

4. *EPMA*

Electron-probe microanalysis investigations of bulk samples reveal that oxygen-deficient regions exist near grain boundaries. However, much more important seems to be the fact, that some regions of the crystallites are also oxygen or oxygen and yttria deficient, whereas the Ba and Cu content of the crystallites turns out to remain almost constant.

C. ac susceptibility

ac susceptibility measurements of the as-prepared crystallites reveal a sharp superconducting transition at 89.4 K (50%) and a transition width of less than 0.6 K (10–90 %). Nevertheless, a small foot is observed. After 7 days of annealing under flowing oxygen at around 400 K no remarkable difference in T_c is detectable and the foot has neither vanished nor even shifted.

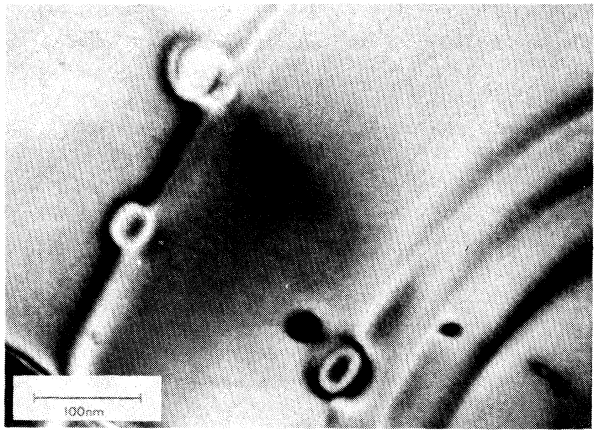

FIG. 4. TEM micrograph of a crystallite. Small inclusions with an average dimension of about 35 nm are visible. Dislocations are seen to be associated with the inclusions.

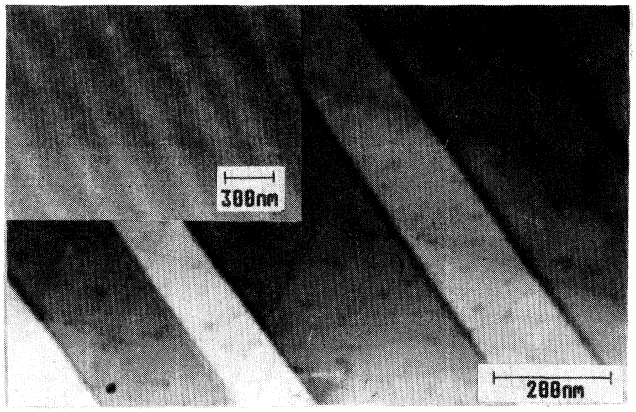

FIG. 6. TEM micrograph showing twin boundaries with an average spacing of about 350 nm. The inset shows a SEM micrograph of the surface of a crystallite recorded with backscattered electrons. Twin boundaries with an average spacing of about 270 nm are visible.

D. Magnetization measurements

Magnetization measurements of the melt-textured samples exhibit a strong hysteresis. At low temperatures the magnetic hysteresis width decreases slowly with increasing temperature and increasing effective magnetic fields, $B_{\text{eff}}=B-\mu_0 DM$ (Fig. 8). At higher temperatures measurements of the magnetization versus B_{eff} exhibit an anomalous behavior. Starting with a decrease of the magnetization hysteresis width with increasing effective magnetic field the hysteresis width increases and after a maximum at an effective magnetic field B^*, which is sometimes higher than the hysteresis width for very small fields, it decreases again (see, e.g., Fig. 9). According to the shape of the anomalous $M(B)$ behavior, it is called fishtail behavior. The second peak in the magnetization curve at B^* shifts with increasing temperature to decreasing effective magnetic fields.[22]

E. Magnetization critical current densities

Applying the Bean critical-state model[15] the magnetic critical current density, $j_{c,\Delta M}$, could be estimated in the case of $B\|c$ using the relation[16]

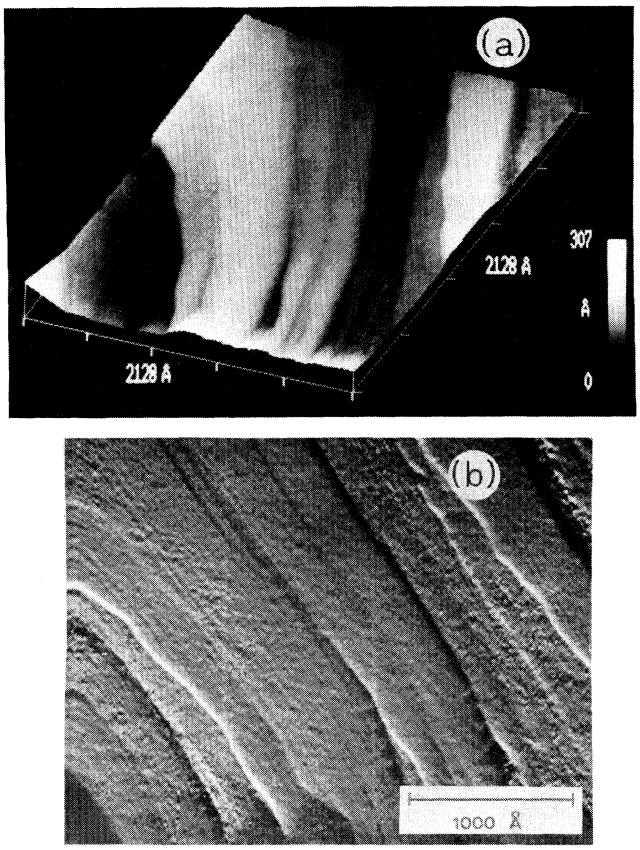

FIG. 7. STM micrograph taken from the surface of a crystallite showing unfiltered raw data in three dimensions (a) and its gradient representation in two dimension (b). Growth steps of height of the elementary unit cell are visible.

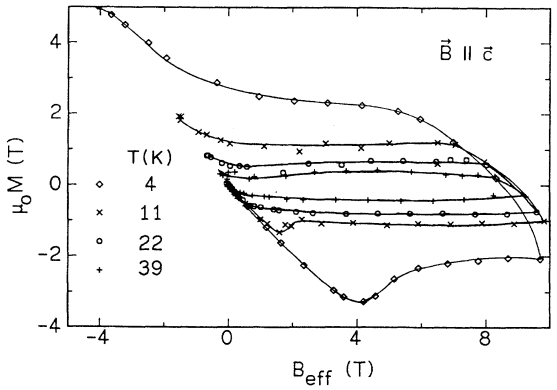

FIG. 8. Zero-field-cooled magnetization curves for $T=4$, 11, 22, and 39 K. The external magnetic field was applied parallel to the c axis.

$$j_{c,\Delta M}(B_{\text{eff}})=\frac{2\Delta M(B_{\text{eff}})}{\mu_0 a(1-a/3b)}\ , \tag{1}$$

where $\Delta M(B_{\text{eff}})$ denotes the width of the magnetization curve at the effective magnetic field B_{eff} and a,b the sample dimensions ($a\le b$) in the plane perpendicular to the external magnetic field direction. Using relation (1) and assuming that the crystallites are "quasi single crystalline" in the a and b directions (see above), $j_{c,\Delta M}$ is estimated to $\sim 2\times 10^6$ A/cm^2 at 4 K and 5 T, and $\sim 4\times 10^4$ A/cm^2 at 70 K and 2 T, respectively (Fig. 10). The pronounced second peak is clearly seen at elevated temperatures.

IV. DISCUSSION

The magnetically measured critical current density, $j_{c,\Delta M}$, of the melt-textured crystallites is about 1 order of magnitude higher than the intragrain critical current

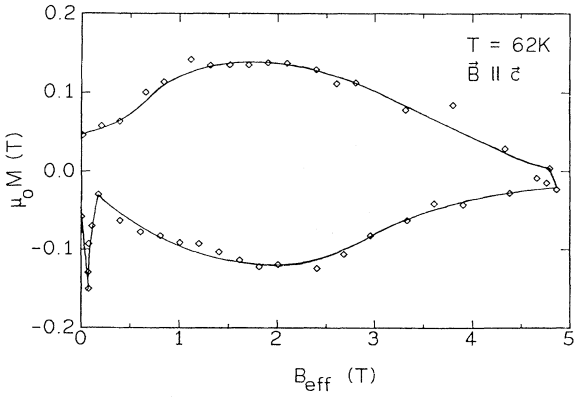

FIG. 9. Magnetization curve at 62 K with **B**$\|$**c**. Prior to the measurement the magnetic field was cycled so as to ensure full penetration of the screening currents.

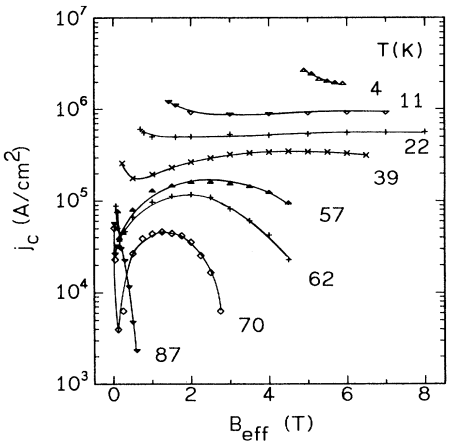

FIG. 10. Field dependence of the critical current density of the crystallites at different temperatures for **B**||**c**.

density of polycrystalline specimens.[23–25] However, one should keep in mind that there are uncertainties in the j_c determination from magnetization measurements due to an ill-defined actual grain size in the case of polycrystalline material. Furthermore, from $\rho(T,B)$ measurements the activation energy, U_0, for thermally activated flux flow is estimated to be almost four times higher in the melt-textured samples than in polycrystalline material.[26] These enhancements could be caused by the presence of the many observed microstructural defects which are absent in polycrystalline samples. It is well known that due to the small coherence length, ξ, of YBCO practically every defect could act as a pinning center but, e.g., grain boundaries could also act as weak links.

Using direct summation, a simple estimation of core pinning[27] by the observed small inclusions yields[26]

$$j_{c,i}=\frac{B_c^2}{4\mu_0 B}\pi\langle\xi\rangle\langle d\rangle N_i \ , \tag{2}$$

where B_c, $\langle\xi\rangle$, $\langle d\rangle$, and N_i denote the thermodynamic critical induction, the average coherence length, $\langle\xi\rangle=(\xi_{ab}^2\xi_c)^{-1/3}$, the average diameter of the inclusions, and their density, respectively. With the above-mentioned values $N_i=6\times10^{19}$ cm^{-3} and $\langle d\rangle=35$ nm and by inserting B_c at 4 K (70 K) = 1.6 T (0.69 T) (Ref. 28) and $\langle\xi\rangle$ at 4 K (70 K) = 0.61 nm (1.2 nm),[29] $j_{c,i}$ at 4 K (70 K) and 5 T (2 T) turns out to be 4.1×10^4 A/cm^2 (3.7×10^4 A/cm^2). Taking into account thermally activated flux motion and the fact that $j_{c,i}$ is overestimated by a direct summation even at 70 K and 2 T this $j_{c,i}$ value is a little too small to explain the measured $j_{c,\Delta M}$ value of $\sim4\times10^4$ A/cm.[2] At 4 K and 5 T this $j_{c,i}$ value of 4.1×10^4 A/cm^2 is far below the measured $j_{c,\Delta M}$ value of $\sim2\times10^6$ A/cm.[2] Thus, other effects must be taken into account.

Assuming that strain fields near the dislocations lower the superconducting (sc) order parameter and that the sc order parameter is zero in the dislocation core as well as that the flux lines are parallel to the dislocation line element, **ds**, one can estimate the pinning potential, U_p, for core pinning by dislocations

$$U_p=\frac{B_c^2}{2\mu_0}\eta V_{WW} \ . \tag{3}$$

In the case of dislocations the interaction volume per unit length of dislocation line, V_{WW}, is assumed conservatively to be about $(\pi/4)|\mathbf{b}^2|$, where **b** denotes the burgers vector. η $(0\le\eta\le1)$ is a factor which takes into account that parts of the dislocation lines are bent too much to allow the flux lines to be pinned along the total dislocation lines. The elementary pinning force is given by

$$f_p=\frac{U_p}{\langle\xi\rangle_\perp} \ , \tag{4}$$

where $\langle\xi\rangle_\perp$ denotes the average coherence length perpendicular to the line element of the dislocation. Because of the high Ginzburg-Landau parameter κ, the constant for flux line lattice shear, c_{66}, is small.[30–33] Thus, the flux line lattice (FLL) in HTSC is very soft. The average distance between the dislocation lines $d_d=N_d^{-1/2}\approx100$ nm is larger than the flux line lattice spacing, a_0, of ~50 nm (~20 nm) at 1 T (5 T). Therefore it is assumed that each dislocation line can pin a flux line. Thus, direct summation is used where the volume pinning force, $F_p=j_cB$, is given by

$$F_p=N_d f_p \ . \tag{5}$$

N_d denotes the dislocation density. The critical current density $j_{c,d}$ for core pinning by dislocations can be determined to

$$j_{c,d}=\eta\pi\frac{B_c^2N_d|\mathbf{b}|^2}{8\mu_0\langle\xi\rangle_\perp B} \ . \tag{6}$$

To estimate the maximum possible $j_{c,d}$ for an orientation of **B** parallel to **c**, the line elements, **ds**, of all dislocations are assumed to lie in the c direction. $\langle\xi\rangle_\perp$ can then be replaced by ξ_{ab}. With the above-mentioned values $N_d=1-2\times10^{10}$ cm^{-2}, $|\mathbf{b}|=3.8$ Å, B_c at 4 K (70 K) = 1.6 T (0.69 T), and ξ_{ab} at 4 K (70 K) = 1.2 nm (2.4 nm), respectively, and assuming 0.8 for η because of the very soft FLL, $j_{c,d}$ at 4 K (70 K) and 5 T (2 T) is estimated to be $2-3\times10^5$ A/cm^2 ($4-7\times10^4$ A/cm^2).

In the case of **ds**⊥**c** and **B**||**c**, the effective interaction volume, $V_{WW_{\text{eff}}}$, is given by $(\pi/4)|\mathbf{b}|^2 2\xi_{ab}$ and the effective density $N_{d_{\text{eff}}}$ by N_d/a_f (for $B>0.25$ T $\rightsquigarrow a_f<N_d^{-1/2}$). Thus, using a similar estimation as above for **ds**⊥**c** and **B**||**c**, Eq. (6) transforms to

$$j_{c,d}=\eta\pi\frac{B_c^2N_d|\mathbf{b}|^2}{4\mu_0 a_f B} \ . \tag{7}$$

Therefore, for an effective magnetic field parallel to the c axis, $j_{c,d}$ for **ds**⊥**c** turns out to be $a_f/(2\xi_{ab})$ times smaller, than for **ds**||**c**, i.e., 5–100 times smaller, depending on the considered field and temperature value.

This is a very crude estimation because direct summation usually yields a too high pinning potential and thermally activated flux motion also has to be taken into

account at higher temperatures. Nevertheless, due to the conservation estimation of the interaction volume, V_{WW}, which could be higher than $(\pi/4)|\mathbf{b}|^2$, dislocations could be strong anisotropic pinning sites.

On the other hand, the strained region surrounding a dislocation could cause the observed fishtail.[22] Another possible origin of the fishtail, as proposed by Daeumling *et al.*,[34] might be the oxygen-deficient regions which were observed by EPMA. The strained regions near the dislocation core as well as oxygen-deficient regions are both thought to possess a lower T_c and B_{c2} compared to the YBCO matrix. Thus, they become pinning centers if the effective external magnetic field becomes higher than their upper critical field. Therefore, a peak in the magnetization curves at finite field is observed, which shifts with decreasing temperature to increasing effective magnetic fields.

The fact that ac susceptibility measurements of as-prepared and oxygen-annealed (7 days, flowing O_2) crystallites show no difference in the transition temperature or the transition width and that a small foot neither vanishes nor even shifts, favor an interpretation where the fishtail is caused by the strained and disordered regions near the dislocation core. In the case of core pinning by dislocations as discussed above, we assume that the strained regions surrounding the dislocations become normal conducting for increasing external magnetic fields and temperatures and therefore that the effective interaction volume $V_{WW_{\text{eff}}}$ becomes temperature and field dependent, i.e., $V_{WW_{\text{eff}}}=\chi(T,B)(\pi/4)|\mathbf{b}|^2$. $\chi(T,B)$ increases with temperature and effective magnetic field $[\chi(T,B)\geq 1]$. In addition, a factor $(1-b^*)$, with $b^*=B/B_{c_2}$, takes into account the decrease of the condensation energy in a magnetic field. Thus, Eq. (6) transforms to

$$j_{c,d}=\eta\chi(T,B)\pi\frac{B_c^2 N_d|\mathbf{b}|^2}{8\mu_0\langle\xi\rangle_\perp B}(1-b^*)\ . \tag{8}$$

This equation allows a qualitative correct description of the observed increase of the hysteresis width with increasing magnetic fields. The decrease of the magnetic hysteresis width for effective magnetic fields greater than $B^*(T)$ is due to the fact that above $B^*(T)$ all strained regions which could become normal conducting are already normal conducting and therefore $\chi(T,B)$ becomes constant.

V. CONCLUSIONS

It was shown that crystallites of melt-textured YBCO possess different kinds of microstructural imperfections. A high density of very fine inclusions of about 6×10^{19} m^{-3} with an average diameter of about 35 nm, a high density of dislocations of about $1-2\times10^{10}$ cm^{-2}, twins, stacking faults, oxygen and yttria deficient regions are as well observed as regular growth steps of height of the YBCO unit cell. The high density of defects improves the pinning strength and explains the enhanced critical current density [e.g., $j_{c,\Delta M}$ (4 K, 5 T) $\approx2\times10^6$ A/cm^2)] compared to polycrystalline intragrain critical current densities [e.g., $j_{c,\Delta M}$ (4 K , 5 T) $\approx2\times10^5$ A/cm^2].[23] An estimation of core pinning by the observed inclusions could neither explain the $j_{c,\Delta M}$ value at 4 K and 5 T nor the increase of $j_{c,\Delta M}$ with increasing effective magnetic field (fishtail) at higher temperatures. Therefore, other defects must be taken into account.

Assuming the core of the dislocation to be nonsuperconducting it was shown that dislocations could cause anisotropic pinning. Strain fields (disordered regions) around the dislocation core which possess a lower T_c and $B_{c_2}(T)$ than the YBCO matrix could result in a temperature- and field-dependent interaction volume and therefore explain the observed fishtail behavior.

ACKNOWLEDGMENTS

The authors would like to thank Professor T. Hehenkamp for the EPMA measurements, G. Kumm for the measurements of the ac susceptibility, and the Solvay Barium Strontium GmbH for the polycrystalline YBCO precursors which were used in the melt-texturing process. This work was supported by the Bundesministerium für Forschung und Technologie (BMFT) under the Grant No. 13N5493A.

[1]S. Jin, T. H. Tiefel, R. C. Sherwood, R. B. van Dover, M. E. Davis, G. W. Kammlot, and R. A Fastnacht, Phys. Rev. B **37**, 7850 (1988).

[2]S. Jin, T. H. Tiefel, R. C. Sherwood, R. B. van Dover, M. E. Davis, G. W. Kammlot, and R. A. Fastnacht, Appl. Phys. Lett. **52**, 2074 (1988).

[3]K. Salama, V. Selvmanickam, L. Gao, and K. Sun, Appl. Phys. Lett. **54**, 2352 (1989).

[4]V. Selvmanickam, and K. Salama, in *High Temperature Superconductors: Fundamental Properties and Novel Materials Processing,* edited by D. K. Christen, J. Narayan, and L. F. Schneemeyer, MRS Symposia Proceedings No. 169 (Materials Research Society, Pittsburgh, 1990), p. 279.

[5]M. Murakami, M. Morita, K. Doi, K. Miyamoto, and H. Hamada, Jpn. J. Appl. Phys. **28**, L1125 (1989).

[6]M. Murakami, Mod. Phys. Lett. B **4**, 163 (1990).

[7]P. J. McGinn, W. Chen, N. Zhu, U. Balachandran, and M. T. Lanagan, Physica C **165**, 480 (1990).

[8]J. Ekin, A. Braginski, A. Panson, M. Janocko, N. Zaluzek, B. Flandermeyer, O. de Lima, M. Homg, J. Kwo, and S. Liou, J. Appl. Phys. **62**, 4821 (1987).

[9]J. Ekin, Adv. Ceram. Mater. **2**, 568 (1987).

[10]M. Murakami, M. Morita, K. Doi, K. Miyamoto, and H. Hamada, Jpn. J. Appl. Phys. **28**, L399 (1989).

[11]M. Murakami, M. Morita, K. Doi, and K. Miyamoto, Jpn. J. Appl. Phys. **28**, 1189 (1989).

[12]M. Murakami, S. Gotoh, N. Koshizuka, S. Tanaka, T. Matsushita, S. Kambe, and K. Kitazawa, Cryogenics **30**, 390 (1990).

[13]M. Murakami, K. Yamaguchi, H. Fujimoto, N. Nakamura, T. Taguchi, N. Koshizuka, and S. Tanaka, Cryogenics **32**, 930 (1992).

[14]M. Ullrich, D. Müller, K. Heinemann, L. Niel, and H. C. Freyhardt, Physica C **198**, 181 (1992).
[15]C. P. Bean, Phys. Rev. Lett. **8**, 250 (1962).
[16]H. P. Wiesinger, F. M. Sauerzopf, and H. W. Weber, Physica C **203**, 121 (1992).
[17]M. Steins, Ph.D. thesis, University of Göttingen, Germany, 1990.
[18]M. Steins, F. Mattheis, R. Gaebel, K. Bente, and H. U. Krebs, J. Cryst. Growth **128**, 772 (1993).
[19]J. Demny, Z. Naturforsch. A **15**, 194 (1960).
[20]S. Nakahara, S. Jin, R. C. Sherwood, and T. H. Tiefel, Appl. Phys. Lett. **54**, 1926 (1989).
[21]D. Müller, M. Ullrich, K. Heinemann, L. Niel, and H. C. Freyhardt (unpublished).
[22]M. Ullrich, D. Müller, K. Heinemann, L. Niel, and H. C. Freyhardt, Appl. Phys. Lett. (to be published).
[23]W. Y. Guan, Y. H. Xu, and K. Zeibig, in *Superconductivity and Applications,* edited by H. S. Kwok (Plenum, New York, 1990), p. 249.
[24]D. Shi, M. S. Boley, J. G. Chen, M. Tang, U. Welp, W. K. Kwok, and B. Malek, Supercond. Sci. Technol. **2**, 255 (1989).
[25]M. R. Cimberle, C. Ferdeghini, G. L. Nicchiotti, M. Putti, A. S. Siri, C. Rizzuto, C. A. Costa, M. Ferretti, C. L. Olcese, F. C. Matacotta, and E. Olzi, Supercond. Sci. Technol. **1**, 30 (1988).
[26]M. Ullrich, D. Müller, K. Heinemann, L. Niel, and H. C. Freyhardt, IEEE Trans. Appl. Supercond. **3**, 1386 (1993).
[27]A. M. Campbell and J. E. Evetts, Adv. Phys. **21**, 199 (1972).
[28]M. Suenaga, D. O. Welch, Y. Xu, Y. Zhu, A. K. Ghosh, and A. R. Moodenbaugh, in *Superconductivity and Applications,* edited by H. S. Kwok (Plenum, New York, 1990), p. 27.
[29]K. Winzer and G. Kum, Z. Phys. B **82**, 317 (1991).
[30]R. Labusch, Phys. Status Solidi **19**, 715 (1967).
[31]R. Labusch, Phys. Status Solidi **32**, 439 (1969).
[32]E. H. Brandt, J. Low Temp. Phys. **26**, 709 (1977).
[33]E. H. Brandt, Phys. Rev. B **37**, 6514 (1986).
[34]M. Daeumling, J. M. Seuntjes, and D. C. Larbalastier, Nature **346**, 332 (1990).

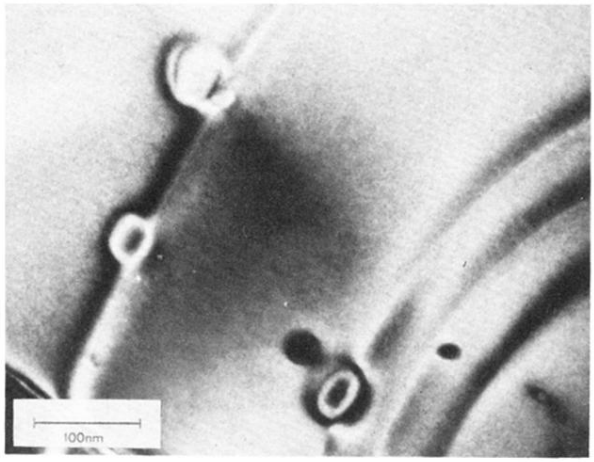

FIG. 4. TEM micrograph of a crystallite. Small inclusions with an average dimension of about 35 nm are visible. Dislocations are seen to be associated with the inclusions.

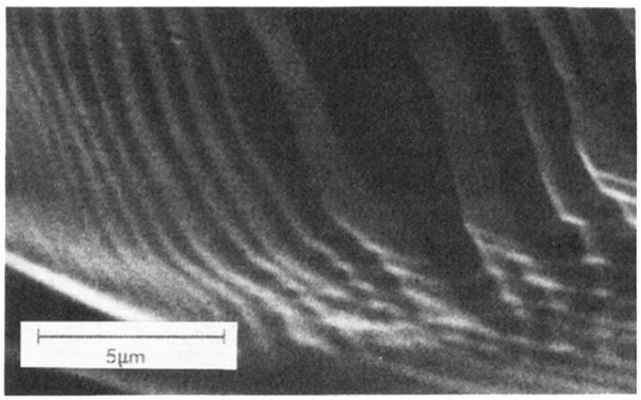

FIG. 5. SEM micrograph of the edge of a crystallite. Large growth steps are visible.

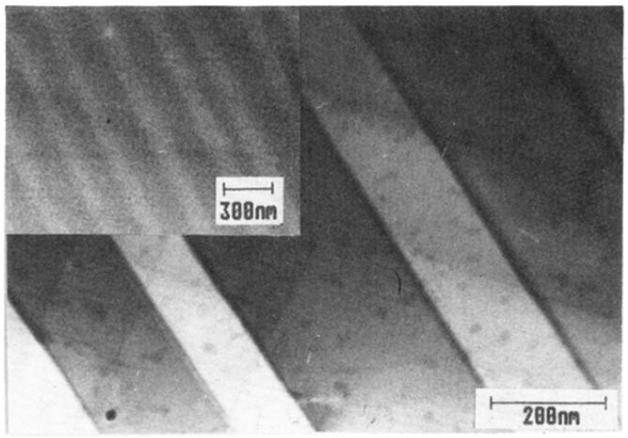

FIG. 6. TEM micrograph showing twin boundaries with an average spacing of about 350 nm. The inset shows a SEM micrograph of the surface of a crystallite recorded with backscattered electrons. Twin boundaries with an average spacing of about 270 nm are visible.

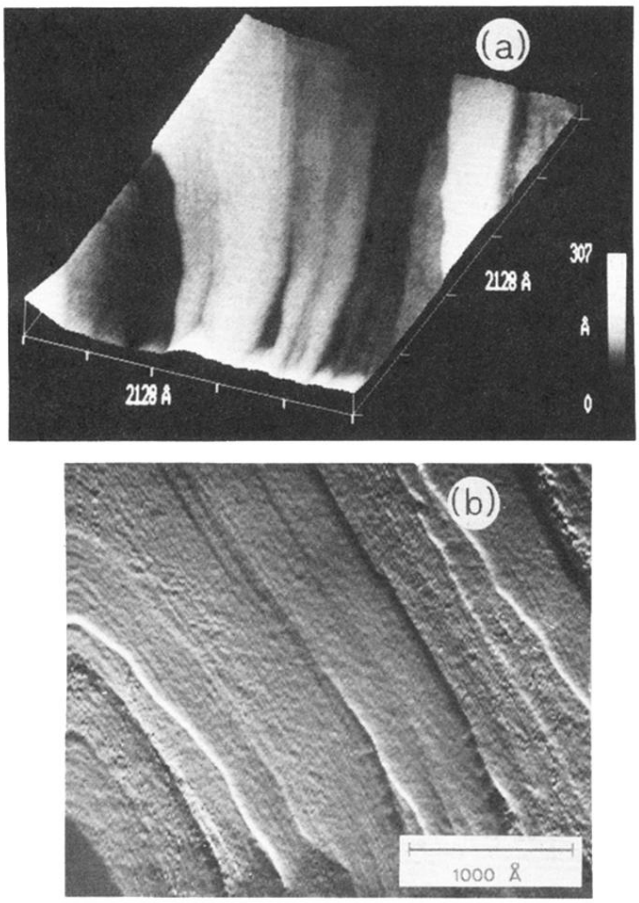

FIG. 7. STM micrograph taken from the surface of a crystallite showing unfiltered raw data in three dimensions (a) and its gradient representation in two dimension (b). Growth steps of height of the elementary unit cell are visible.